論文の内容の要旨

The study of warm molecular gas in the vicinity of active galactic nuclei with the near-infrared CO absorption band

（一酸化炭素近赤外線吸収バンドを用いた活動銀河核近傍の高温分子ガスの研究）

氏名　　馬場　俊介

An active galactic nucleus (AGN) is a galactic central region that exhibits intense activity being powered by mass accretion onto a supermassive black hole. Its energy output plays a significant role in the formation and evolution of the host galaxy. This central engine is considered to be surrounded by a dusty structure like a torus (AGN torus). The anisotropy of the torus is a key factor in understanding widely diverging appearances of AGNs. When an AGN is observed from the direction parallel to its torus axis, broad optical emission lines that originate from the vicinity of the nucleus are directly seen, and the AGN is recognized as type-1. When the AGN is viewed from the direction perpendicular to the axis, the broad lines are obscured by the extinction within the torus, only narrow optical emission lines originating from a region above the torus are observed, and the AGN is recognized as type-2. This viewing angle effect is the fundamental concept of the unification scheme of AGNs. Many modifications and extensions of this basic picture have been proposed to explain complicated characteristics of AGNs with different luminosities and multi-wavelength properties. In any case, at least it is certain that some anisotropic structure exists at the center of an AGN. For the establishment of a unified understanding of AGNs, it is essential to observe and investigate physical states and structures of AGN tori in a large sample including AGNs of different properties. However, the small parsec-scale sizes of AGN tori make it tough to perform spatially-resolved direct observations.

The strategy in this thesis is near-infrared spectroscopy of the CO fundamental rotational-vibrational absorption band centered at 4.67 μm. A schematic picture of this method is shown in Figure 1. If a torus is viewed edge-on, using the bright near-infrared dust emission from the central region as the background continuum, we can expect to observe the foreground torus with an effectively high spatial resolution owing to the compactness of the continuum source. The aim of this thesis is to demonstrate the effectiveness of the CO absorption as a probe of a putative AGN torus and use it to investigate torus properties in galaxies of different luminosities and optical classifications. The Infrared Camera (IRC) onboard the AKARI satellite enables unique observations of the CO absorption even in less-luminous galaxies of infrared luminosities of 10^{11} $L_{\odot}$ or less. Its near-infrared grism spectroscopy covers wavelengths from 2.5 to 5.0 μm with a spectral resolution of about 100 and has a 1σ sensitivity of 0.5 mJy.

However, the IRC near-infrared spectrum is problematic at wavelengths longer than 4.9 μm being contaminated by the diffracted second-order light, which prevents the accurate flux calibration in that range. To utilize the IRC observations for our study, we corrected for the effect of the contamination.

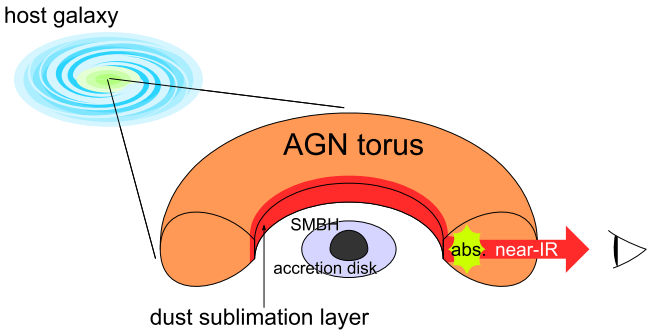

Figure 1: Schematic picture of the observation method of the near-IR absorption spectroscopy.

First, we fixed the artifact in the observations that had been conducted during the cryogenic phase of the satellite. The IRC wavelength calibration was revised by considering a higher-order effect caused by the wavelength dependence of the refractive index of the grism material. The new wavelength calibration revealed that the contamination occurs due to the nonlinearity arising from the refractive index, even if the order-sorting filter coated on the grism perfectly cuts off wavelengths shorter than 2.5 μm. The spectral responses from the first- and second-order light were simultaneously obtained by using standard objects of red and blue spectra, which leads contrastive strengths of the contamination. With the new responses, the first- and second-order light mixing in 4.9–5.0 μm were quantitatively decomposed for the first time.

We then proceeded to the post-cryogenic phase, during which the detector temperature had gradually increased. The revised wavelength calibration curve in the post-cryogenic phase was found to be consistent with that in the cryogenic phase and not to have any significant temperature dependence. The response from the first-order light was found to be smaller than that in the cryogenic phase by a factor of 0.7. The decline of the response during the period was evaluated to be 10%. The relative strength of the contaminating second-order light to the first-order spectrum was found to be smaller than that in the cryogenic phase by 25%, reflecting the degradation of the point-spread function around 2.5μm relevant to the contaminated range.

Next, using spectroscopic observations with the *AKARI* and *Spitzer* satellites, we analyzed band profiles of the CO absorption in nearby ten AGNs, which had been known to show the feature, by fitting a plane-parallel local thermal equilibrium gas model. The results are shown in Figure 2. The CO gas was found to be warm (200–500 K) and to have a large column density ($N_{\rm H} \gtrsim 10^{23}$ cm^{-2}) as shown in Figure 3. The heating of the gas is not explicable by either UV heating or shock heating because these processes cannot represent the observed large column densities. Instead, X-ray radiation from the nuclei is the most convincing candidate because it can produce large columns of warm gas of up to $N_{\rm H} \sim 10^{24}$ cm^{-2}. Based on the adoption of the CO abundance of CO/H $= 10^{-4}$, the hydrogen column density estimated from the CO band was smaller than that inferred from X-ray observations. These results can be explained that the region probed by the near-infrared CO absorption is in the vicinity of the nuclei and is located outside the X-ray emitting region. Furthermore, the almost unity covering factors required by the observed deep absorption profiles suggest that the probed region is close to the continuum source, which can be designated as the inner rim of the obscuring material around the AGNs.

Being motivated by the above result, we performed a systematic analysis of the CO band with a larger sample that includes less-luminous infrared galaxies. Nearby 47 infrared galaxies were selected from the *AKARI* post-cryogenic observations without any prior information on the presence or absence of the CO feature. Their band profiles were compared in different luminosity classes and optical classifications. Many of the sample galaxies showed warm large-column gas of $N_{\rm CO} \gtrsim 10^{19}$ cm^{-2} and $T_{\rm CO} \sim$ several $\times\, 10^2$ K, which can be considered to be heated by X-rays. High-luminosity galaxies ($> 10^{11}$ $L_\odot$) showed deeper absorption profiles than less-luminous galaxies ($< 10^{11}$ $L_\odot$) as shown in Figure 4. We found that the fraction of galaxies with $N_{\rm CO} > 10^{19}$ cm^{-2} had a peak at a 14 μm monochromatic luminosity of 10^{10} $L_\odot$ as shown in Figure 5, being consistent with the obscured fraction measured in X-ray observations. Based on this result, the obscuring material observed in X-rays is being identified to be molecular gas. We also found that AGN-starburst composites had on average larger $N_{\rm CO}$ than Seyfert 2 galaxies. This result can be interpreted that the obscuration by an AGN torus is also effective in composites and that the torus is geometrically thicker in composites than in typical Seyfert galaxies. This picture is qualitatively consistent with the connection that supernovae in the circum-nuclear disk inflate the scale height of the torus.

Our studies indicate that warm molecular gas with a large column density exists in the vicinity of AGNs and that such gas has properties common to the obscuring material observed in X-rays. These results suggest that the anisotropic structure around an AGN consists of molecular gas, agreeing with the AGN unified model.

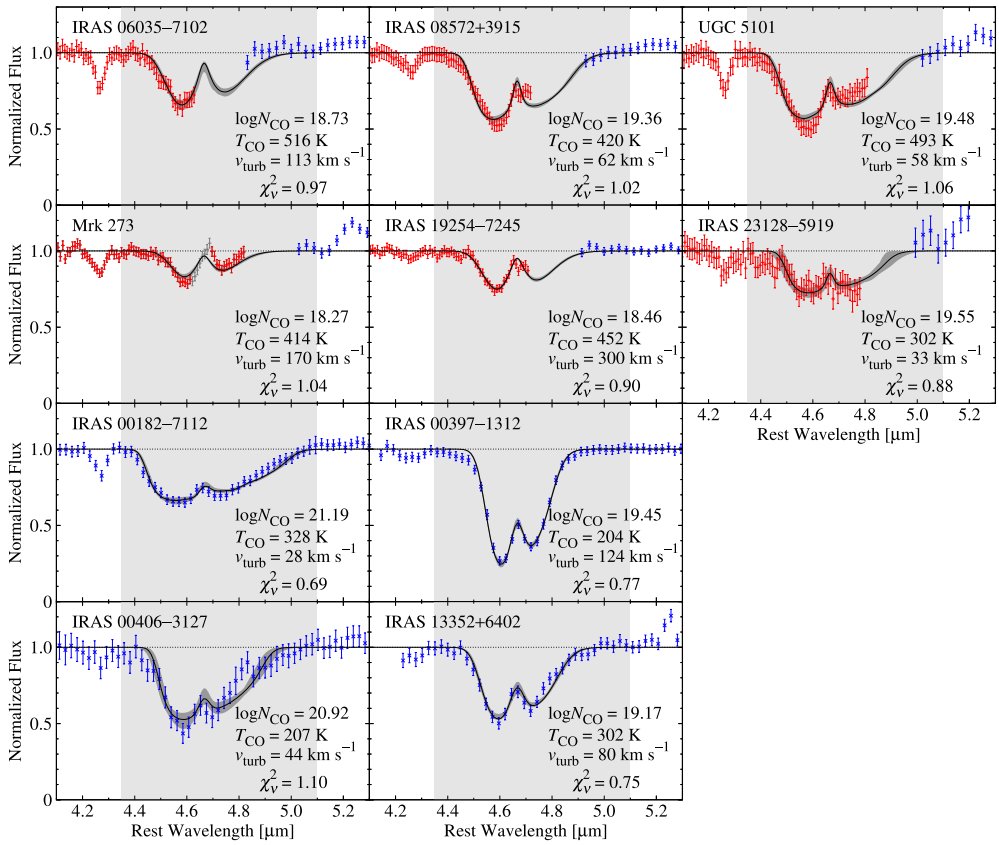

Figure 2: Black solid lines denote the best-fit CO absorption profiles, and the accompanying gray-filled curves represent the intervals corresponding to the 68% joint confidence level. Red and blue points are data from the *AKARI*/IRC and *Spitzer*/IRS spectra, respectively. Gray shaded areas indicate the wavelength range used for the spectral fitting. Dark-gray points in the spectrum of Mrk 273 were excluded from the fitting to avoid the possible contribution from the Pfβ (4.65 μm) emission. The best-fit values for the CO column density $N_{\rm CO}$, temperature $T_{\rm CO}$, and turbulent velocity $v_{\rm turb}$, and the goodness-of-fit $\chi^2_\nu \equiv \chi^2/{\rm dof}$ are noted at the right bottom corners.

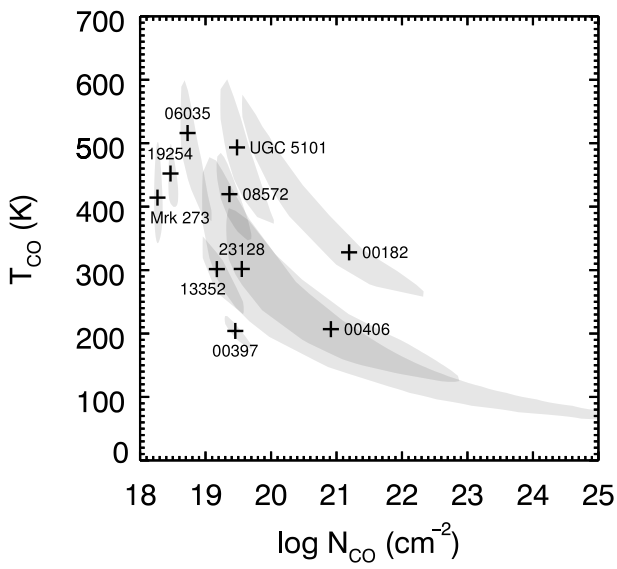

Figure 3: Plot of $T_{\rm CO}$ versus $N_{\rm CO}$. Black points indicate the best-fit values. Gray shaded areas are the projection of the three-dimensional 68% joint confidence regions along the $v_{\rm turb}$ axis.

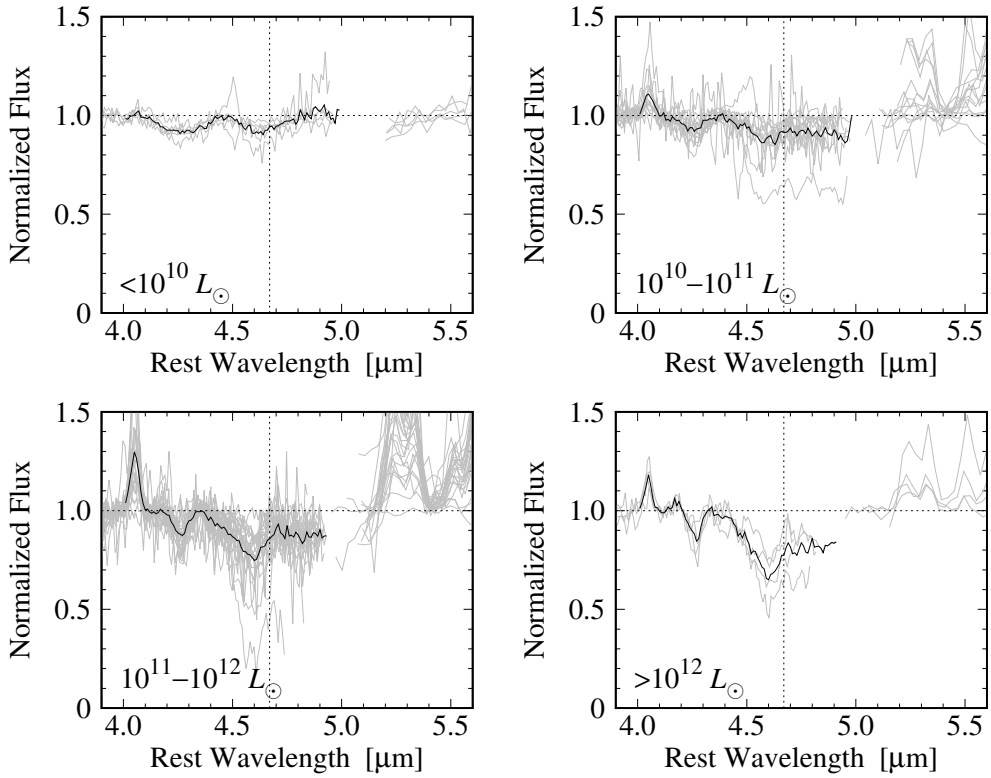

Figure 4: Observed CO absorption profiles divided by classes of the infrared luminosity. Gray lines represent individual spectra, and black lines show the average in the classes. Only the data from *AKARI* were used for the average.

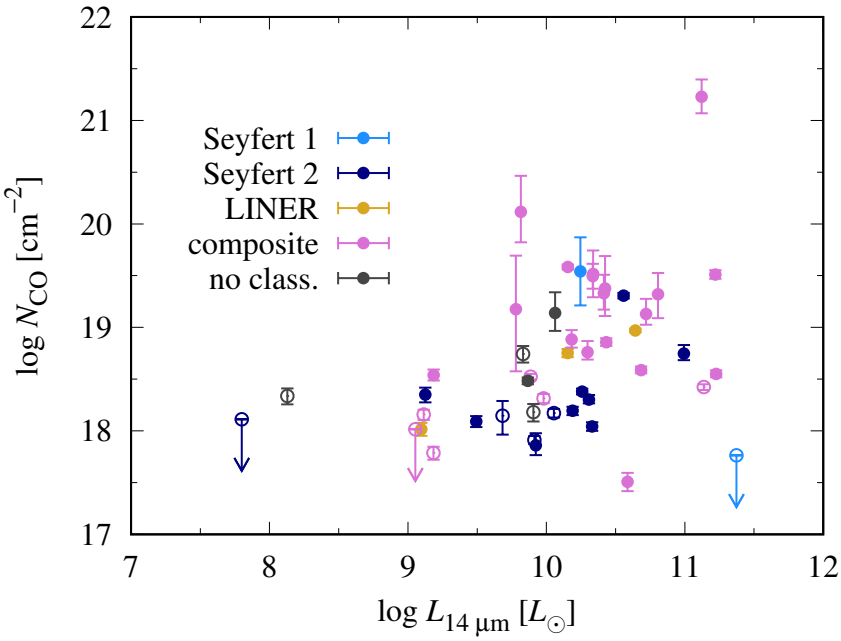

Figure 5: Plot of $N_{\rm CO}$ against the 14 μm monochromatic luminosity $L_{14\,\mu{\rm m}}$. Filled and open points represent the results from the fitting with $v_{\rm turb}$ fixed and from that with both $v_{\rm turb}$ and $T_{\rm CO}$ fixed, respectively. Error bars represent the 68% joint confidence range.